
Dehazing Light Microscopy Images with Guided Conditional Flow Matching: *finding a sweet spot between fidelity and realism*

Anirban Ray^{1,2}, Ashesh^{1,2}, and Florian Jug¹

¹Human Technopole, Milan, Italy

²Technische Universität Dresden, Germany

{anirban.ray, ashesh.ashesh, florian.jug}@fht.org

Abstract

Fluorescence microscopy is a major driver of scientific progress in the life sciences. Although high-end confocal microscopes are capable of filtering out-of-focus light, cheaper and more accessible microscopy modalities, such as widefield microscopy, can not, which consequently leads to hazy image data. Computational dehazing is trying to combine the best of both worlds, leading to cheap microscopy but crisp-looking images. The perception-distortion trade-off tells us that we can optimize either for data fidelity, e.g. low MSE or high PSNR, or for data realism, measured by perceptual metrics such as LPIPS or FID. Existing methods either prioritize fidelity at the expense of realism, or produce perceptually convincing results that lack quantitative accuracy. In this work, we propose HAZEMATCHING, a novel iterative method for dehazing light microscopy images, which effectively balances these objectives. Our goal was to find a balanced trade-off between the fidelity of the dehazing results and the realism of individual predictions (samples). We achieve this by adapting the conditional flow matching framework by guiding the generative process with a hazy observation in the conditional velocity field. We evaluate HAZEMATCHING on 5 datasets, covering both synthetic and real data, assessing both distortion and perceptual quality. Our method is compared against 7 baselines, achieving a consistent balance between fidelity and realism on average. Additionally, with calibration analysis, we show that HAZEMATCHING produces well-calibrated predictions. Note that our method does not need an explicit degradation operator to exist, making it easily applicable on real microscopy data. All data used for training and evaluation and our code will be publicly available under a permissive license.

1 Introduction

Today, inverse problems in computer vision are often addressed with deep learning approaches of various sorts (Liu et al. [2021]), and image dehazing is one such inverse problem that has important applications in the life sciences. When imaging biological samples with a light microscope, diffraction limited 2D images can be acquired. The focal depth of such images can vary greatly, depending on the microscopy modality to be used: confocal microscopes have an exquisitely shallow depth of focus, leading to very crisp images subject to little haze, while widefield microscopes have a much wider depth of focus and are therefore collecting large amounts of out-of-focus light, leading to hazy images that are harder to interpret and analyze. Confocal microscopes achieve their high image quality via optical sectioning with a physical pinhole in the light path of the microscope. While this is a fantastic optical trick, it has also downsides, one of which is the price of such microscopes.

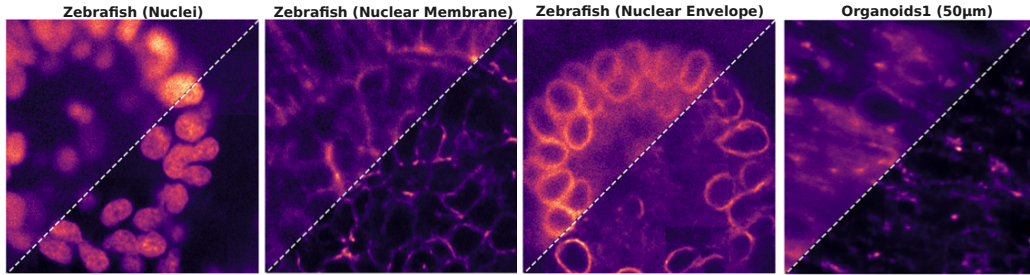


Figure 1: **Teaser:** Our method, HAZEMATCHING, proposes a way to utilize Conditional Flow Matching to remove out-of-focus light (haze) from biomedical microscopy data.

Here, we ask the question to what degree can we replace the optical ingenuity of confocal microscopes by purely computational means. If a body of hazy widefield microscopy images is given to us, can we devise a method that can solve the inverse task of predicting how the same sample would appear if it were imaged with a confocal microscope?

Natural choices for tackling the inverse task of dehazing are supervised setups (Ronneberger et al. [2015], Sønderby et al. [2016]), or diffusion-like setups (Delbracio and Milanfar [2023]), or flow matching approaches ([Albergo et al., 2024]). In all cases, we require a body of paired data, *i.e.* pairs of images that show the same image content (the biological sample $s \in S$), once with and another time without haze. Technically, this can be achieved by acquiring data at a confocal microscope (non-hazy images) and acquiring a second micrograph after fully opening the above-mentioned pinhole (leading to widefield-like hazy images). Another possibility is to use synthetically generated microscopy images, using a microscopy simulator that simulates the optics of various light microscopes. In this work, we do both – we use synthetic data, giving us precise control and full knowledge of s , and we use real microscopy data to demonstrate that our method works on real microscopy data.

While computational dehazing enables life scientists to use cheaper, faster, and less photon-toxic microscopes while still obtaining crisp images for downstream analyses, the perception–distortion trade-off must be considered [Blau and Michaeli, 2018, Shroff et al., 2024]. We can optimize either for data fidelity (*e.g.*, low MSE or high PSNR) or for perceptual realism (*e.g.*, low LPIPS or FID), but not both simultaneously. Supervised networks trained with conservative losses such as MSE or MAE preserve fidelity by staying close to the evidence in the given input data, while generative methods like diffusion or flow matching favor realism by aligning predictions with the target domain (haze-free images). Since both objectives cannot be optimized simultaneously, one must choose based on the application. In scientific imaging, our stance is clear: the fidelity to the raw data (our scientific measurements) is the most important.

However, powerful generative models may produce visually convincing but scientifically inaccurate results, favoring target domain realism over fidelity. In this work, we explore alternatives to traditional MSE/MAE-based training and leverage recent advances in flow matching, particularly the concept of stochastically interpolant flow matching with data-dependent coupling (SIFM) [Albergo et al., 2024].

2 Related Work

Classical deconvolution methods such as Richardson–Lucy (RL) efficiently reverse optical blur in fluorescence and confocal microscopy but amplify noise and depend on explicit point spread function (PSF) models and full 3D stacks, often introducing artifacts (Lucy [1974], Liu et al. [2025]). Learning-based point predictors, notably U-NET trained with MSE introduced in Weigert et al. [2018], Krull et al. [2019], capture multiscale context and improve restoration quality but produce oversmoothed outputs (Delbracio and Milanfar [2023]). Variational approaches such as hierarchical VAEs (HVAE) and their microscopy adaptations enable uncertainty-aware sampling from learned posteriors (Sønderby et al. [2016], Prakash et al. [2022]), but remain single-pass and cannot iteratively refine predictions. Iterative generative methods like diffusion models (Ho et al. [2020], Song et al. [2021], Kawar et al. [2022]) and conditional flow matching (CFM) (Lipman et al. [2023]) progressively denoise to recover sharp structures; diffusion achieves state-of-the-art restoration at the

cost of slow inference and fixed degradation assumptions (Saharia et al. [2021], Bansal et al. [2022]). While CFM’s ODE-based transport offers faster, deterministic sampling, it is still underexplored for microscopy image restoration, with recent efforts like (Albergo et al. [2024]) highlighting its potential.

2.1 Overview: Conditional Flow Matching (CFM)

Conditional Flow Matching (CFM) is a method for training continuous-time generative models, where a neural network learns a time-dependent vector field that transports samples from a base distribution to a target data distribution. Here, we present a brief recap of flow matching and its relation to conditional flow matching.

Let $p_0(x)$ and $p_1(x)$ be the base and target data distributions respectively. The goal of Flow Matching is to learn a continuous-time transport map that evolves samples from p_0 into samples from p_1 . This transport is represented by a family of mappings $\psi_t(x_0)$ for $t \in [0, 1]$ with ψ_t being the mapping function and $x_0 \sim p_0(x)$, and the evolution is governed by a time-dependent vector field $v^t(x)$ such that

$$\frac{d}{dt}\psi_t(x_0) = v^t(\psi_t(x_0)), \quad \psi_0(x_0) = x_0. \quad (1)$$

The density of transformed samples at time t , denoted by the probability density function p_t , is the pushforward of p_0 under ψ_t , i.e., $p_t = (\psi_t)_\# p_0$. Here $\#$ is the pushforward operator which describes how the distribution p_0 changes to p_t when its random variables are transformed by ψ_t . Lipman et al. [2023] introduced a simulation-free method to train such a vector field by minimizing a regression loss

$$\min_{\theta} \mathbb{E}_{t \sim \mathcal{U}[0,1], x \sim p_t} \|v_{\theta}^t(x) - v^t(x)\|^2, \quad (2)$$

where v_{θ}^t is the learnable vector field, and $v^t(x)$ is the *target* vector field that generates the intermediate distributions p_t connecting p_0 to p_1 , subject to the boundary conditions $p_{t=0} = p_0$ and $p_{t=1} = p_1$. Since computing p_t and v^t directly is intractable in general, Lipman et al. [2023] proposed a conditional formulation. Rather than modeling the marginals p_t and the marginal vector field $v^t(x)$, one can model the *conditional* path $p_t(x|x_1)$ and *conditional* vector field $v^t(x|x_1)$, where $x_0 \sim p_0(x)$ and $x_1 \sim p_1(x)$ are coupled. In particular, one can define a deterministic interpolation path between x_0 and x_1 with ψ_t as

$$\psi_t(x_0|x_1) = x_t = (1-t)x_0 + tx_1, \quad (3)$$

and define the conditional velocity field along this path as

$$v^t(x_t|x_1) = \frac{dx_t}{dt} = x_1 - x_0. \quad (4)$$

This leads to the Conditional Flow Matching (CFM) objective

$$\min_{\theta} \mathbb{E}_{t \sim \mathcal{U}[0,1], x_0 \sim p_0, x_1 \sim p_1} \|v_{\theta}^t(x_t) - (x_1 - x_0)\|^2. \quad (5)$$

2.2 Data-dependent realizations of CFM

When applying CFM to image restoration, conditioning on the observation is essential to ensure consistency with the input, distinguishing it from purely generative tasks. While recent diffusion and CFM methods address related problems, they are not directly suited for dehazing. For instance, Lee et al. [2023] propose learning a data-dependent coupling over $p_1(x_1)p_0(x_0|x_1)$ via a forward model $q_{\theta}(x_0|x_1)$, where $x_0 \sim \mathcal{N}(\mu_{\theta}(x_1), \Sigma_{\theta}(x_1))$. Although this imposes a Gaussian degradation conditioned on x_1 , it lacks dependence on external observations (e.g., hazy images), preventing guided sampling. At inference, x_0 must be sampled from $\mathcal{N}(0, I)$, making the method unsuitable for tasks like dehazing or deconvolution where control over the input is critical.

Similarly, SIFM Albergo et al. [2024] proposes to define an explicit data-dependent coupling between x_0 and x_1 by introducing a degradation operator $m(x_1)$, leading to the base sample x_0 through $x_0 = m(x_1) + \sigma\zeta$, where $\zeta \sim \mathcal{N}(0, I)$ and $\sigma > 0$. This method is effective when the degradation operator m and noise level σ are known or reliably estimated. However, in microscopy, m is typically unknown, and noise properties vary widely. Even with access to $m(x_1)$ during training, generating multiple samples at inference is non-trivial without an accurate noise level estimate. Arbitrary choices of σ risk distribution mismatch between training and inference, which is problematic for scientific

applications. While adding synthetic noise during training is a potential solution, microscopy data already contains significant noise from photon shot noise and detector imperfections (Photonics, Bankhead), making this approach detrimental. In our experiments, we refer to this baseline as $\text{SIFM}\{\sigma_a|b\}$, where a and b denote the σ used during training and inference, respectively, and $a, b \in \mathbb{R}$.

To address the challenges of applying Conditional Flow Matching (CFM) to image dehazing, we propose **HAZEMATCHING**, a novel framework that formulates dehazing as a guided conditional transport problem. We model stochastic interpolation between noisy, hazy (source), and non-hazy (target) image distributions, bridging observed haze and the underlying scene. We extend CFM with degradation-aware conditioning to guide the flow using hazy inputs. Our iterative design enables diverse, high-fidelity predictions crucial for microscopy, and supports posterior sampling. We further perform uncertainty calibration and show that **HAZEMATCHING** produces well-calibrated predictions, where error correlates with predicted variance. Overall, it achieves a balanced trade-off between *perceptual quality* and *distortion* compared to baselines.

3 Methods

3.1 Problem definition

The forward model that describes how hazy microscopy images are formed is described by $\mathbf{x}_M = H_M(s) + \eta(s)$, where H_M is the unknown hazing function for a microscope M , s is the true signal, *i.e.* the imaged 3D sample, η is a noise function that can depend on the true signal, and \mathbf{x}_M is the hazy observed image. Depending on M , the used microscope, the observed image \mathbf{x}_M will contain different levels of signal-dependent haze. For example, for a widefield microscope M_0 and a confocal microscope M_1 , we can image two micrographs

$$\mathbf{x}_{M_0} = H_{M_0}(s) + \eta(s), \quad (6)$$

$$\mathbf{x}_{M_1} = H_{M_1}(s) + \eta(s), \quad (7)$$

Using microscopes M_0 and M_1 we can therefore acquire sets of images X_0 and X_1 according to Equations 6 and 7, respectively. Let S be a set of biological samples s_i defined as

$$S = \{s^i | i = 1, 2, \dots, N\}, \quad N \in \mathbb{N}. \quad (8)$$

An image $\mathbf{x}_M^i \in X_{j \in \{0,1\}}$ can be seen as being drawn from a distribution of images $\mathbf{x}_{M_j}^i \sim p_{M_j}(\mathbf{x} | s^i)$ where p_{M_j} is the distribution of images acquired at the microscope j . Note that M_0 and M_1 generate images that are subject to a very different amount of haze, where $\mathbf{x}_{M_0}^i \sim p_{M_0}(\mathbf{x} | s^i)$ belong to the hazy image domain and corresponding $\mathbf{x}_{M_1}^i \sim p_{M_1}(\mathbf{x} | s^i)$ belong to the domain of non-hazy micrographs. With this in mind, the task of *image dehazing* is to predict

$$\hat{\mathbf{x}}_{M_1}^i = D(\mathbf{x}_{M_0}^i), \quad (9)$$

where D is a function that solves the dehazing task, and $\hat{\mathbf{x}}_{M_1}^i$ is *close* to the unknown $\mathbf{x}_{M_1}^i$. We will later discuss in detail what ‘close’ means in the context of this work.

The ambition of **HAZEMATCHING** is, given training data X_0 and X_1 to learn a D that will allow microscopist to acquire images with more accessible, cheaper and less photon-toxic widefield microscopes M_0 and use the learned D to predict images close to those imaged with expensive confocal microscopes such as M_1 .

3.2 Our approach

Our goal is to learn a function D that maps a hazy microscopy image to its corresponding non-hazy version, leveraging paired data acquired from two imaging modalities M_0 and M_1 . To model this translation, we adopt the Conditional Flow Matching (CFM) framework, which constructs a continuous path from Gaussian noise to the clean image $\mathbf{x}_{M_1} \sim p_{M_1}(\mathbf{x} | s^i)$, while conditioning the learned velocity field on the degraded input $\mathbf{x}_{M_0} \sim p_{M_0}(\mathbf{x} | s^i)$. This allows the model to learn a data-driven transport map that reconstructs high-fidelity structure informed by low-quality observations.

3.2.1 Marginal probability path for the dehazing task

Let us start by defining our initial distributions. We have samples from three distributions to work with – **Noisy image distribution**: $\mathbf{x}_0 \sim \mathcal{N}(0, I)$ which is our base distribution which we denote as $p_0(\mathbf{x})$. Note that in our text, we use the notations $p_0(\mathbf{x})$ and $\mathcal{N}(0, I)$ interchangeably. **Source image distribution (hazy)** $\mathbf{x}_{M_0} \sim p_{M_0}(\mathbf{x}|s^i)$ which is our degraded observation for which we want to learn a non-hazy version and, **Target image distribution (non-hazy)** $\mathbf{x}_{M_1} \sim p_{M_1}(\mathbf{x}|s^i)$.

For our supervised learning setup, we draw each pair $(\mathbf{x}_{M_0}, \mathbf{x}_{M_1})$ corresponding to observations of an underlying biological sample s^i from a set of samples S as shown in equation 8. The joint distribution over all variables, conditioned on the sample s^i , is

$$p(\mathbf{x}_0, \mathbf{x}_{M_0}, \mathbf{x}_{M_1} | s^i) = p_0(\mathbf{x}_0) p_{M_0}(\mathbf{x}_{M_0}^i | s^i) p_{M_1}(\mathbf{x}_{M_1}^i | s^i). \quad (10)$$

Given this setup, we define a linear interpolation path \mathbf{x}_t (as shown in equation 3) between the noise sample $\mathbf{x}_0 \sim \mathcal{N}(0, I)$ and the clean target image \mathbf{x}_{M_1} as

$$\mathbf{x}_t = (1 - t)\mathbf{x}_0 + t\mathbf{x}_{M_1}, \quad \text{for } t \in [0, 1]. \quad (11)$$

Since \mathbf{x}_0 is independent Gaussian noise, the resulting marginal probability density path p_t over the interpolant \mathbf{x}_t , conditioned on the clean image \mathbf{x}_{M_1} , is a Gaussian (Lipman et al. [2023]) described as

$$p_t(\mathbf{x} | \mathbf{x}_{M_1}) = \mathcal{N}(t\mathbf{x}_{M_1}, (1 - t)^2 I); \quad \mathbf{x}_t \sim p_t(\mathbf{x} | \mathbf{x}_{M_1}). \quad (12)$$

3.2.2 Marginal velocity field for the dehazing task

In the standard CFM framework (see Section 2.1), the conditional velocity field is defined as $v^t(\mathbf{x}_t | \mathbf{x}_{M_1})$, where \mathbf{x}_{M_1} is the clean image available during training, which makes the marginal velocity field, as shown by Lipman et al. [2024], of the form

$$v^t(\mathbf{x}_t) = \int v^t(\mathbf{x}_t | \mathbf{x}_{M_1}) p_{M_1}(\mathbf{x}_{M_1} | \mathbf{x}_t) d\mathbf{x}_{M_1}. \quad (13)$$

However, in our framework, the conditional velocity field explicitly depends not only on the interpolant \mathbf{x}_t but also on the degraded observation \mathbf{x}_{M_0} and takes the form $v^t(\mathbf{x}_t, \mathbf{x}_{M_0} | \mathbf{x}_{M_1})$. Therefore, we extend the formulation presented in Lipman et al. [2024], where the marginal velocity field then takes the form of

$$v^t(\mathbf{x}_t, \mathbf{x}_{M_0}) = \int v^t(\mathbf{x}_t | \mathbf{x}_{M_1}, \mathbf{x}_{M_0}) p_{M_1}(\mathbf{x}_{M_1} | \mathbf{x}_t, \mathbf{x}_{M_0}) d\mathbf{x}_{M_1}. \quad (14)$$

This formulation clearly illustrates the conditional dependency on the degraded observation \mathbf{x}_{M_0} , which is essential for accurately transporting the sample \mathbf{x}_0 to \mathbf{x}_{M_1} guided by the hazy image \mathbf{x}_{M_0} . Thus, to solve the dehazing task through $v^t(\mathbf{x}_t, \mathbf{x}_{M_0})$, we adapt the standard CFM framework (equation 5) to guided CFM framework, to accommodate our per-sample unique guidance. We train a neural network v_θ^t to approximate v^t by minimizing the objective parameterized by θ as

$$\min_{\theta} \mathbb{E}_{(\mathbf{x}_0, \mathbf{x}_{M_0}, \mathbf{x}_{M_1}), \mathbf{x}_t} \|v_\theta^t(\mathbf{x}_t, \mathbf{x}_{M_0}) - (\mathbf{x}_{M_1} - \mathbf{x}_0)\|^2, \quad (15)$$

where $(\mathbf{x}_0, \mathbf{x}_{M_0}, \mathbf{x}_{M_1}) \sim p(\mathbf{x}_0, \mathbf{x}_{M_0}, \mathbf{x}_{M_1} | s^i)$ and $\mathbf{x}_t \sim p_t(\mathbf{x} | \mathbf{x}_{M_1})$. This results in a learned velocity field which models the conditional transport from \mathbf{x}_0 to $\hat{\mathbf{x}}_{M_1}$ guided by \mathbf{x}_{M_0} .

The inference procedure then becomes our $D(\mathbf{x}_{M_0})$ which solves the dehazing task, as described in equation 9. The function D then comprises of v_θ^t which is our trained velocity predictor and an ODE solver. To perform dehazing with D , we start with a given hazy observation $\mathbf{x}_{M_0} \sim p_{M_0}(\mathbf{x})$. We then sample an independent $\mathbf{x}_0 \sim \mathcal{N}(0, I)$ and concatenate $\mathbf{x}_0, \mathbf{x}_{M_0}$ along the channel dimension and use the learned velocity field $v_\theta^t(\mathbf{x}_0, \mathbf{x}_{M_0})$ to predict the velocity $(d\mathbf{x}_t/dt)$ for each $t \in [0, 1]$ described as

$$\frac{d\mathbf{x}_t}{dt} = v_\theta^t(\mathbf{x}_0, \mathbf{x}_{M_0}). \quad (16)$$

We then integrate the predicted velocities from $t = 0$ to $t = 1$ using the (Euler) ODE solver to predict the non-hazy image at $t = 1$. Note that we can generate multiple samples by repeating this process and the desired stochasticity comes from sampling a new $\mathbf{x}_0 \sim \mathcal{N}(0, I)$ for each prediction. The detailed training and dehazing procedure by D are given in Algorithm 1 and Algorithm 2, respectively.

Algorithm 1 HAZEMATCHING: Training

Require: Initialized velocity model v_θ^t , learning rate γ .
Require: List of predefined time steps $\{t_i\}_{i=0}^N \subset [0, 1]$ ▷ with $t_0 = 0, t_N = 1$
1: **repeat**
2: Sample: $\mathbf{x}_0 \sim \mathcal{N}(0, I), \mathbf{x}_{M_0} \sim p_{M_0}(\mathbf{x}|s^i), \mathbf{x}_{M_1} \sim p_{M_1}(\mathbf{x}|s^i)$
3: Sample $t \sim \mathcal{U}\{t_i\}$
4: Compute $\mathbf{x}_t = (1-t)\mathbf{x}_0 + t\mathbf{x}_{M_1}$ ▷ see equation 11
5: Compute Loss: $\mathcal{L} = \|v_\theta^t(\mathbf{x}_t, \mathbf{x}_{M_0}) - (\mathbf{x}_{M_1} - \mathbf{x}_0)\|^2$ ▷ see equation 15
6: $\theta \leftarrow \theta - \gamma \nabla_\theta \mathcal{L}$
7: **until** training has converged
8: **Return** v_θ^t

Algorithm 2 HAZEMATCHING: Sampling with dehazing function D

Require: Hazy image $\mathbf{x}_{M_0}^i$, Trained network v_θ^t
Require: Number of integration steps $T \in \mathbb{N}$
1: Compute step size $\delta = 1/T$
2: Draw $\mathbf{x}_0 \sim \mathcal{N}(0, I)$
3: **for** $t = 1$ to T **do**
4: $\mathbf{x}_t = \mathbf{x}_{t-1} + \delta \cdot v_\theta^{\delta(t-1)}(\mathbf{x}_t, \mathbf{x}_{M_0}^i)$ ▷ with Euler ODE integration
5: **end for**
6: **Return** \mathbf{x}_T as the non-hazy prediction $\hat{\mathbf{x}}_{M_1}^i$

3.3 Calibrated uncertainty in the predictions

In addition to the evaluations in Section 4, we integrate an uncertainty calibration module to assess prediction reliability. A network is considered well-calibrated when predicted uncertainties align with actual errors, allowing users to assess confidence directly. Although calibration by design is ideal, it is often not achieved (Guo et al. [2017]). To address this, a suitable transformation can be applied to align uncertainties with observed errors. Ideally, a calibration plot should closely follow the line $y = x$, where y denotes the error and x the predicted uncertainty. The calibration procedure follows `MicroSplit` (Ashesh et al. [2025]), using a learned mapping to align predicted uncertainties with observed errors. We visualize calibration quality by plotting RMSE versus RMV across bins. A well-calibrated model yields a curve that aligns closely with the $y = x$ line. In our results, we report the uncalibrated and calibrated plot alongside the learned α (denoted as the `Scaling factor`) and β (denoted as the `Offset`) values.

4 Experiments

We evaluate our method on five datasets. Below we describe the three datasets we decided to show in the main paper.

Zebrafish data: We use zebrafish retina images taken at a confocal microscope available from Weigert et al. [2018] and simulated haze on top of it. We use `microsim` Lambert [2022] to simulate haze in microscopy images. The dataset consist of nuclei, nuclear membrane and nuclear envelope. We train and evaluate all of these structures in a single model. There are a total of 15 training images and 3 images each of val and test all of shape (1024×1024) .

Organoids1 and Organoids2 data: These are real microscopy data acquired as pairs on a spinning-disk and confocal microscope, respectively. The haze effect in the confocal is achieved by fully opening the pinhole and the clean image is acquired at using a 1 AU pinhole diameter. For the spinning-disk, we have removed the entire disk of pinholes to obtain the hazy widefield image. Organoids1 and Organoids2, each have 15 training images 3 test and 2 val images all of shape (1024×1024) .

Training: We use 128×128 patches for training. All models are trained setting $T=20$ integration steps, using a U-NET [Dhariwal and Nichol, 2021] in PyTorch [Paszke et al., 2017] on an NVIDIA

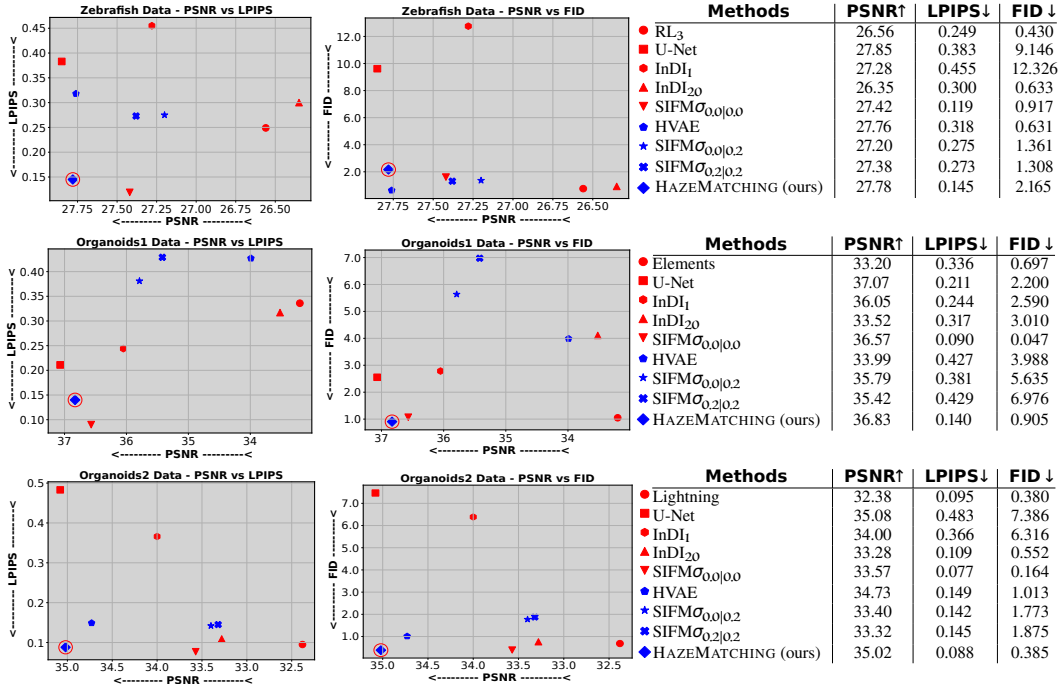


Figure 2: **Data fidelity vs. realism.** Each row corresponds to one dataset, *i.e.* *Zebrafish* (top), *Organoids1* (middle), and *Organoids2* (bottom). For each dataset, we show PSNR vs. LPIPS (left) and PSNR vs. FID (center), capturing the trade-off between pixel-level fidelity and perceptual quality. Our goal is to find a method that leads to high fidelity (high PSNR) while also leading to realistic looking predictions (low LPIPS/FID). (HAZEMATCHING is highlighted with an additional red circle.) Results tables (right) further summarize our results. Note that HAZEMATCHING consistently achieves balanced performance across all metrics and datasets. Methods displayed in red are point-predicting baselines, while blue methods are generative posterior models (see main text).

V100 GPU. The torchCFM [Tong, 2024] library is used for interpolant computation and ODE integration.

Evaluation: We use both, *distortion metrics* (via PSNR [Weigert et al., 2018], MicroMS-SSIM [Ashesh et al., 2024] on full frame predictions computed using inner tiling Ashesh et al. [2023]) and *perceptual quality metrics* (via LPIPS [Zhang et al., 2018] and FID [Heusel et al., 2017] on non-overlapping 64×64 patches).

Baselines: We compare our results against classical Richardson–Lucy (RL) deconvolution [Lucy, 1974], deterministic point-predicting models (U-NET [Ronneberger et al., 2015] and InDI₁ in single step prediction mode [Delbracio and Milanfar, 2023]), and a variational HVAE [Sønderby et al., 2016] baseline. Additionally, we also compare against iterative methods, *i.e.* InDI₂₀ (20 steps of generating diverse predictions. For *Organoids1* and *Organoids2*, we additionally compare against proprietary software *Elements* from Nikon Instruments Inc. and *Lightning* from Leica Microsystems, respectively.

5 Results

Perception–distortion trade-off: Our main evaluation focuses on the trade-off between distortion and perceptual quality. To this end, we plot LPIPS vs. PSNR and FID vs. PSNR in Figure 2), jointly assessing content fidelity (PSNR) and perceptual quality (LPIPS, FID). We do prefer models having high PSNR and low LPIPS/FID, which in our plot are located closer to the bottom left. HAZEMATCHING consistently achieves a favorable balance, outperforming deterministic baselines in perceptual quality, while remaining competitive with the best fidelity-optimized generative posterior

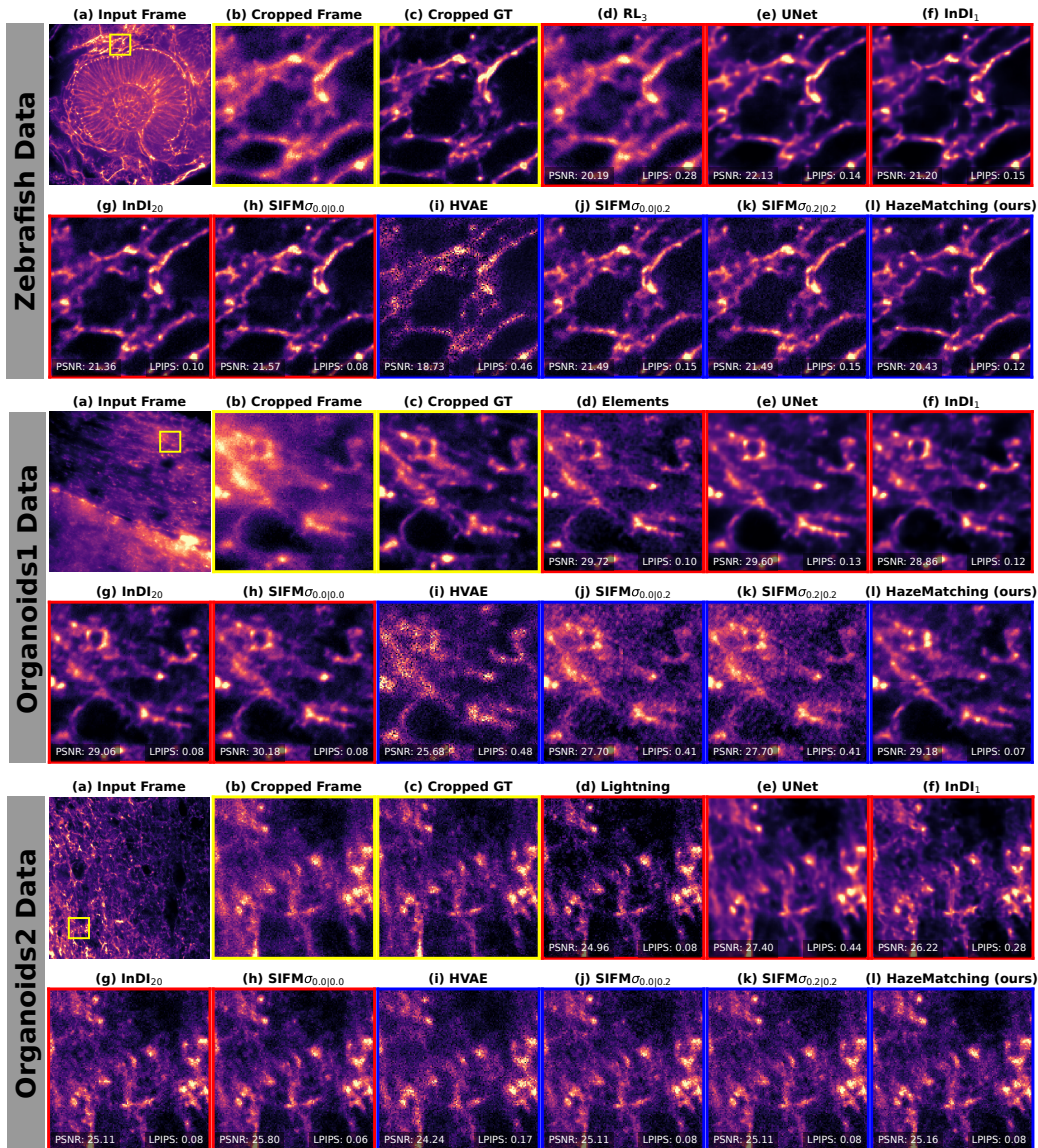


Figure 3: **Qualitative results.** We show representative results for three dataset. For each dataset we show (a) the full input and a selected crop (yellow box), (b) the selected crop, (c) non-hazy ground truth, (d–k) predictions by all baseline methods (see Section 4), and (l) results obtained with HAZEMATCHING. Results with red borders are predictions by point-predictors, while methods with blue borders are results by generative posterior models (see also Figure 2 and main text).

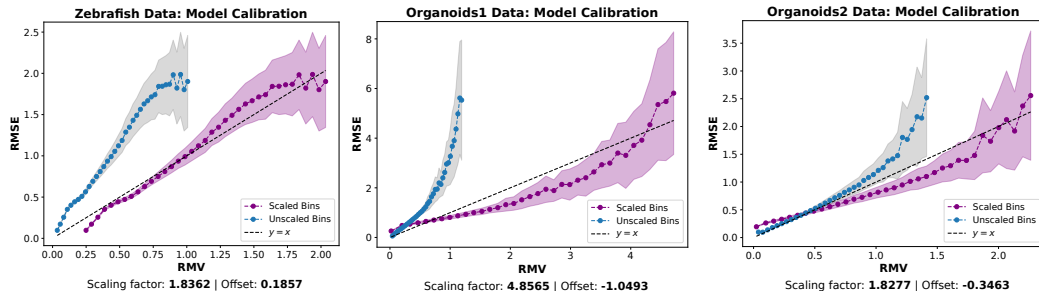


Figure 4: **Calibration of HAZEMATCHING.** RMSE vs. predicted RMV is shown for *Zebrafish*, *Organoids1*, and *Organoids2* (left to right). The dashed line indicates ideal calibration ($y = x$). Blue and purple circles show uncalibrated and calibrated results, respectively, with shaded areas denoting standard error. Calibration parameters (scaling and offset) are shown below each plot.

baselines. Posterior models (blue markers) generate diverse and realistic looking outputs; point predictors (red) yield single predictions. For posterior models, we report the PSNR of an approximate MMSE (average of 50 samples) and average of the per-sample LPIPS and FID scores.

Calibration analysis: We assess how HAZEMATCHING deals with data uncertainty by conducting a calibration analysis on predicted variance maps. In Figure 4 we plot RMSE vs. RMV (root mean variance) for the three main datasets ($y=x$ shown as a dashed line). Note that our trained models are well calibrated, suggesting that we can use the variability in posterior samples as a surrogate for the true prediction error.

Qualitative comparisons: In Figure 3 we show representative results for the three main datasets, with PSNR and LPIPS reported on a highlighted crop. Red and blue outlines indicate whether a model is a point-predictors or a posterior model, respectively. Deterministic models tend to predict overly smooth results, while posterior models, especially HAZEMATCHING, produce sharper, more realistic looking outputs. Still, HAZEMATCHING does not sacrifice data fidelity, which is in-line with our initial goal.

6 Discussion and Conclusion

HAZEMATCHING addresses a key challenge in microscopy image prediction by enabling realistic, diverse, and well-calibrated predictions under hazy degradations. Unlike MMSE-based models that oversmooth high-frequency details (in a single step), HAZEMATCHING preserves fidelity while producing perceptually realistic predictions. Using CFM, it models the posterior over non-hazy images (in an iterative fashion) given hazy inputs, supporting uncertainty-aware restoration. Experiments across real and simulated datasets show that HAZEMATCHING achieves a favorable perception–distortion trade-off, outperforming deterministic and other posterior (and iterative) baselines in perceptual metrics (LPIPS, FID) while remaining competitive in distortion metric (PSNR). Unlike point predictors, it generates multiple high-quality diverse samples and provides calibrated pixel-wise uncertainty estimates aligned with prediction errors, critical for downstream biological tasks. Evaluations across five datasets confirm its robustness and generalizability under varying noise, resolution, and structural complexity, indicating strong potential for practical deployment. Overall, HAZEMATCHING proposes an iterative image dehazing method extending the CFM framework and provides access to multiple samples under data uncertainty.

Limitations: HAZEMATCHING requires multiple forward passes for diverse samples, increasing inference time. Controlling output diversity remains challenging, and the need for paired data limits use in some scenarios. Broader evaluations on other modalities (e.g., electron microscopy) are needed. Future work may explore efficient sampling, unpaired training, and cross-modality generalization.

In conclusion, HAZEMATCHING bridges the gap between restoration quality and uncertainty modeling in microscopy dehazing, and opens up new possibilities for integrating such methods into practical imaging workflows. We hope this work inspires further research on interpretable, distribution-aware models for scientific imaging domains.

7 Conclusion

In this work, we introduced HAZEMATCHING, a guided Conditional Flow Matching (CFM) based image dehazing method designed for microscopy data. By leveraging CFM, our approach learns to sample from the posterior distribution over non-hazy images given a hazy input, enabling both high-quality dehazing and meaningful uncertainty estimates. Unlike traditional point-prediction models that prioritize pixel-wise accuracy, HAZEMATCHING balances fidelity with perceptual realism, producing diverse outputs that better reflect the underlying distribution of plausible solutions. We demonstrated the effectiveness of our method across five microscopy datasets, showing consistent improvements over deterministic and generative baselines in both perceptual (LPIPS, FID) and distortion (PSNR, MS-SSIM) metrics. Furthermore, our model offers calibrated uncertainty estimates that align well with prediction error, providing a valuable tool for applications requiring reliable confidence quantification. HAZEMATCHING bridges the gap between restoration quality and uncertainty modeling in microscopy dehazing, and opens up new possibilities for integrating such methods into practical imaging workflows. We hope this work inspires further research on interpretable, distribution-aware models for scientific imaging domains.

Acknowledgments and Disclosure of Funding

Our sincere thanks to Francesca Casagrande (Imaging Unit, National Facility for Light Imaging, Human Technopole), Ilaria Laface, and Dario Ricca (Tissue Processing Unit, National Facility for Light Imaging, Human Technopole) for the brain organoid tissue sections we used. We want to thank Jacopo Zasso (National Facility for Genome Engineering and Disease Modeling, Human Technopole) for providing the used brain organoid samples that have been stained by Alessandra Fasciani (Imaging Unit, National Facility for Light Imaging, Human Technopole). Francesca Casagrande also performed the deconvolution of hazy images using *Lightning* and *Elements* software. Image acquisition was carried out by Francesca Casagrande and Alessandra Fasciani (Imaging Unit, National Facility for Light Imaging, Human Technopole). Richardson–Lucy (RL) deconvolution was performed by Eugenia Cammarota (Bioimage Analysis Unit, National Facility for Data Handling & Analysis, Human Technopole). We would also like to acknowledge the support by Talley Lambert (Harvard Medical School) and Vera Galinova (Human Technopole) for their support in setting up the *microsim* pipeline we used and the entire Jug Group for encouraging and enlightening discussions. This work was supported by the European Commission through the Horizon Europe program (IMAGINE project, grant agreement 101094250-IMAGINE and AI4Life project, grant agreement 101057970-AI4LIFE) and the generous core funding of Human Technopole.

References

- Michael Samuel Albergo, Mark Goldstein, Nicholas Matthew Boffi, Rajesh Ranganath, and Eric Vanden-Eijnden. Stochastic interpolants with data-dependent couplings. In Ruslan Salakhutdinov, Zico Kolter, Katherine Heller, Adrian Weller, Nuria Oliver, Jonathan Scarlett, and Felix Berkenkamp, editors, *Proceedings of the 41st International Conference on Machine Learning*, volume 235 of *Proceedings of Machine Learning Research*, pages 921–937. PMLR, 21–27 Jul 2024. URL <https://proceedings.mlr.press/v235/albergo24a.html>.
- Ashesh Ashesh, Alexander Krull, Moises Di Sante, Francesco Pasqualini, and Florian Jug. usplit: Image decomposition for fluorescence microscopy. In *Proceedings of the IEEE/CVF International Conference on Computer Vision (ICCV)*, pages 21219–21229, October 2023. URL https://openaccess.thecvf.com/content/ICCV2023/html/Ashesh_uSplit_Image_Decomposition_for_Fluorescence_Microscopy_ICCV_2023_paper.html.
- Ashesh Ashesh, Joran Deschamps, and Florian Jug. Microsim: Improved structural similarity for comparing microscopy data, 2024. URL <https://arxiv.org/abs/2408.08747>.
- Ashesh Ashesh, Federico Carrara, Igor Zubarev, Vera Galinova, Melisande Croft, Melissa Pezzotti, Daozheng Gong, Francesca Casagrande, Elisa Colombo, Stefania Giussani, Elena Restelli, Eugenia Cammarota, Juan Manuel Battagliotti, Nikolai Klena, Moises Di Sante, Gaia Pigino, Elena Taverna, Oliver Harschnitz, Nicola Maghelli, Norbert Scherer, Damian Edward Dalle Nogare, Joran Deschamps, Francesco Pasqualini, and Florian Jug. Microsplit: Semantic unmixing of fluorescent microscopy data. *bioRxiv*, 2025. doi: 10.1101/2025.02.10.637323. URL <https://www.biorxiv.org/content/early/2025/02/11/2025.02.10.637323>.

- Pete Bankhead. Noise · analyzing fluorescence microscopy images with imagej. https://petebankhead.gitbooks.io/imagej-intro/content/chapters/formation_noise/formation_noise.html. Accessed: 2025-05-04.
- Arpit Bansal, Eitan Borgnia, Hong-Min Chu, Jie S. Li, Hamid Kazemi, Furong Huang, Micah Goldblum, Jonas Geiping, and Tom Goldstein. Cold diffusion: Inverting arbitrary image transforms without noise, 2022. URL <https://arxiv.org/abs/2208.09392>.
- Yochai Blau and Tomer Michaeli. The perception-distortion tradeoff. In *2018 IEEE Conference on Computer Vision and Pattern Recognition, CVPR 2018, Salt Lake City, UT, USA, June 18-22, 2018*, pages 6228–6237. Computer Vision Foundation / IEEE Computer Society, 2018. doi: 10.1109/CVPR.2018.00652. URL http://openaccess.thecvf.com/content_cvpr_2018/html/Blau_The_Perception-Distortion_Tradeoff_CVPR_2018_paper.html.
- Mauricio Delbracio and Peyman Milanfar. Inversion by direct iteration: An alternative to denoising diffusion for image restoration. *Trans. Mach. Learn. Res.*, 2023, 2023. URL <https://openreview.net/forum?id=VmyFF51L3F>.
- Prafulla Dhariwal and Alex Nichol. Diffusion models beat gans on image synthesis, 2021. URL <https://arxiv.org/abs/2105.05233>.
- Chuan Guo, Geoff Pleiss, Yu Sun, and Kilian Q. Weinberger. On calibration of modern neural networks. In *Proceedings of the 34th International Conference on Machine Learning*, volume 70 of *Proceedings of Machine Learning Research*, pages 1321–1330. PMLR, 2017. URL <https://proceedings.mlr.press/v70/guo17a.html>.
- Martin Heusel, Hubert Ramsauer, Thomas Unterthiner, Bernhard Nessler, and Sepp Hochreiter. Gans trained by a two time-scale update rule converge to a local nash equilibrium. In *Advances in Neural Information Processing Systems (NeurIPS)*, pages 6626–6637, 2017.
- Jonathan Ho, Ajay Jain, and Pieter Abbeel. Denoising diffusion probabilistic models. In H. Larochelle, M. Ranzato, R. Hadsell, M.F. Balcan, and H. Lin, editors, *Advances in Neural Information Processing Systems*, volume 33, pages 6840–6851. Curran Associates, Inc., 2020. URL https://proceedings.neurips.cc/paper_files/paper/2020/file/4c5bcfec8584af0d967f1ab10179ca4b-Paper.pdf.
- Bahjat Kawar, Michael Elad, Stefano Ermon, and Jiaming Song. Denoising diffusion restoration models, 2022. URL <https://arxiv.org/abs/2201.11793>.
- Alexander Krull, Tomas Vicar, and Florian Jug. Probabilistic noise2void: Unsupervised content-aware denoising, 06 2019.
- Talley Lambert. microsim: A physics-based confocal and widefield microscopy simulator. <https://talleylambert.com/microsim/>, 2022. Accessed: 2025-05-04.
- Sangyun Lee, Beomsu Kim, and Jong Chul Ye. Minimizing trajectory curvature of ode-based generative models. *arXiv preprint arXiv:2301.12003*, 2023.
- Leica Microsystems. Obtain Maximum Information from Your Specimen with LIGHTNING. <https://www.leica-microsystems.com/science-lab/life-science/obtain-maximum-information-from-your-specimen-with-lightning/>. Accessed: 2025-05-04.
- Yaron Lipman, Ricky T. Q. Chen, Heli Ben-Hamu, Maximilian Nickel, and Matthew Le. Flow matching for generative modeling. In *The Eleventh International Conference on Learning Representations*, 2023. URL <https://openreview.net/forum?id=PqvMRDCJT9t>.
- Yaron Lipman, Marton Havasi, Peter Holderrieth, Neta Shaul, Matt Le, Brian Karrer, Ricky T. Q. Chen, David Lopez-Paz, Heli Ben-Hamu, and Itai Gat. Flow matching guide and code, 2024. URL <https://arxiv.org/abs/2412.06264>.
- Yiming Liu, Spozmai Panezai, Yutong Wang, and Sjoerd Stallinga. Noise amplification and ill-convergence of richardson-lucy deconvolution. *Nature Communications*, 16, 01 2025. doi: 10.1038/s41467-025-56241-x.
- Zhichao Liu, Luhong Jin, Jincheng Chen, Qiuyu Fang, Sergey Ablameyko, Zhaozheng Yin, and Yingke Xu. A survey on applications of deep learning in microscopy image analysis. *Computers in Biology and Medicine*, 134:104523, 2021. doi: 10.1016/j.compbiomed.2021.104523.
- L. B. Lucy. An iterative technique for the rectification of observed distributions. *The Astronomical Journal*, 79: 745, 1974. doi: 10.1086/111605.

- Nikon Instruments Inc. NIS-Elements Imaging Software. <https://www.microscope.healthcare.nikon.com/products/software/nis-elements>. Accessed: 2025-05-04.
- Adam Paszke, Sam Gross, Soumith Chintala, Gregory Chanan, Edward Yang, Zachary DeVito, Zeming Lin, Alban Desmaison, Luca Antiga, and Adam Lerer. Automatic differentiation in pytorch. In *NIPS-W*, 2017.
- Hamamatsu Photonics. What is photon shot noise? https://camera.hamamatsu.com/jp/en/learn/technical_information/thechnical_guide/photon_shot_noise.html. Accessed: 2025-05-04.
- Mangal Prakash, Mauricio Delbracio, Peyman Milanfar, and Florian Jug. Interpretable unsupervised diversity denoising and artefact removal. In *International Conference on Learning Representations*, 2022. URL <https://openreview.net/forum?id=DfMq1BOPXjM>.
- Olaf Ronneberger, Philipp Fischer, and Thomas Brox. U-net: Convolutional networks for biomedical image segmentation. In Nassir Navab, Joachim Hornegger, William M. Wells III, and Alejandro F. Frangi, editors, *Medical Image Computing and Computer-Assisted Intervention - MICCAI 2015 - 18th International Conference Munich, Germany, October 5 - 9, 2015, Proceedings, Part III*, volume 9351 of *Lecture Notes in Computer Science*, pages 234–241. Springer, 2015. doi: 10.1007/978-3-319-24574-4_28. URL https://doi.org/10.1007/978-3-319-24574-4_28.
- Chitwan Saharia, Jonathan Ho, William Chan, Tim Salimans, David J Fleet, and Mohammad Norouzi. Image super-resolution via iterative refinement. *arXiv:2104.07636*, 2021.
- Hari Shroff, Ilaria Testa, Florian Jug, and Suliana Manley. Live-cell imaging powered by computation. *Nature Reviews Molecular Cell Biology*, 25, 02 2024. doi: 10.1038/s41580-024-00702-6.
- Casper Kaae Sønderby, Tapani Raiko, Lars Maaløe, Søren Kaae Sønderby, and Ole Winther. Ladder variational autoencoders. In Daniel D. Lee, Masashi Sugiyama, Ulrike von Luxburg, Isabelle Guyon, and Roman Garnett, editors, *Advances in Neural Information Processing Systems 29: Annual Conference on Neural Information Processing Systems 2016, December 5-10, 2016, Barcelona, Spain*, pages 3738–3746, 2016. URL <https://proceedings.neurips.cc/paper/2016/hash/6ae07dcb33ec3b7c814df797cbda0f87-Abstract.html>.
- Jiaming Song, Chenlin Meng, and Stefano Ermon. Denoising diffusion implicit models. In *International Conference on Learning Representations*, 2021. URL <https://openreview.net/forum?id=St1giarCHLP>.
- Alexander Y. Tong. Torchcfm: A conditional flow matching library, 2024. URL <https://github.com/atong01/conditional-flow-matching>. Accessed: 2025-05-04.
- Martin Weigert, Uwe Schmidt, Tobias Boothe, Andreas Müller, Alexandr Dibrov, Akanksha Jain, Benjamin Wilhelm, Deborah Schmidt, Coleman Broaddus, Siân Culley, Mauricio Rocha-Martins, Fabián Segovia-Miranda, Caren Norden, Ricardo Henriques, Marino Zerial, Michele Solimena, Jochen Rink, Pavel Tomancak, Loïc Royer, Florian Jug, and Eugene W. Myers. Content-aware image restoration: Pushing the limits of fluorescence microscopy. *bioRxiv*, 2018. doi: 10.1101/236463. URL <https://www.biorxiv.org/content/early/2018/07/03/236463>.
- Richard Zhang, Phillip Isola, Alexei A Efros, Eli Shechtman, and Oliver Wang. The unreasonable effectiveness of deep features as a perceptual metric. In *Proceedings of the IEEE Conference on Computer Vision and Pattern Recognition (CVPR)*, pages 586–595, 2018.